Schrödinger wave functions in strong periodic potentials with applications to atom optics

M. Horne,[1] I. Jex,[2,3] and A. Zeilinger[3]
[1]*Stonehill College, North Easton, Massachusetts 02357*
[2]*Department of Physics, Fakulta Jaderna a Fyzikalne Inzenyrska Ceske Vysoke Uceni Technicke, Břehová 7, 115 19 Praha 1, Staré Město, Czech Republic*
[3]*Institut für Experimentalphysik, Universität Innsbruck, Technikerstrasse 25, A-6020 Innsbruck, Austria*
(Received 1 April 1998)

When an atom diffracts in intense standing light, the periodic potential can be too strong for known solutions of the Schrödinger equation. We present general solutions of Schrödinger's equation in strong sinusoidal media, thus generalizing dynamical diffraction theory. The solutions exhibit rich generalizations of the pendellösung phenomena. [S1050-2947(99)01203-2]

PACS number(s): 03.75.Be

I. INTRODUCTION

The quantum mechanics of particle propagation in spatially periodic media has a rich history going back to the 1920s. A standard example of such a system is the diffraction of particles in crystal lattices [1–3]. It exhibits several fascinating features of quantum mechanics. Namely, it illustrates the wave nature of the Schrödinger amplitude and reveals that this amplitude can extend coherently over macroscopic distances. These features enable us, for instance, to construct matter wave interferometers. The basic matter wave effects were demonstrated long ago for electrons, later for neutrons, and recently for atoms. While for electrons and neutrons the periodic medium is usually in the form of a crystal lattice, for atoms the periodic medium is often realized in the form of a standing light wave [4]. It might seem that such a change in experimental realization does not present much that is fundamentally new and does not call for a new theoretical analysis: One simply applies to the atoms the relevant solutions of the Schrödinger equation previously developed for electrons and/or neutrons. However, we find that the potential that a standing light wave presents to an atom is sufficiently different in strength and other significant ways that the needed solutions do not exist in the literature.

Let us take a look at the potential experienced by an atom in a standing light wave [5]

$$V(x,z)=\frac{d^2E^2(x,z)}{\hbar(\Delta+i\gamma/2)}, \tag{1}$$

where x and z are spatial coordinates on the scattering plane of the atom, $E(x,z)$ is the electric field intensity, d is the dipole matrix element of the atom, Δ is the detuning between the light and the atomic transition, and γ is the damping constant of the atom for the unobserved levels. We consider an idealized scheme of a three-level atom. The atom has the ground and excited levels. The third level is the decay level of the excited state. Due to the structure of Eq. (1), we can prepare the medium in various forms. We can make the potential $V(x,z)$ real, imaginary, or generally complex by tuning the light frequency relative to the transition frequency of the atom. We can tailor the periodic medium into an almost arbitrary geometric configuration with the proper optics. As a special example of geometry we mention the problem of the edge of the light beam. By a suitable arrangement, the edge of the light crystal can be made sharp (as we are accustomed to with ordinary crystals) or it can be made soft, enabling an adiabatic penetration of the atom wave into the periodic medium. The potential can be modulated in time, thereby opening the door to many time-dependent phenomena. Most of the listed features are very difficult or impossible to realize with ordinary crystals and thereby make the system of the atom wave and light crystal a unique and in a sense superior system.

A significant additional difference between the potential encountered by an atom in a light crystal and the potential encountered by a neutron in an ordinary crystal is the *strength*. As we shall see below, the crucial dimensionless parameter in Bragg diffraction is q, the ratio of the height of the potential peaks to the transverse (i.e., perpendicular to the lattice plane) kinetic energy of the particle. For Bragg diffracting neutrons $q\simeq 10^{-5}$; for Bragg diffracting atoms in light crystals Eq. (1) reveals that q can be adjusted continuously from zero to 10 or more by simply using brighter light. The existing solutions of Schrödinger's equation used to describe neutron diffraction in crystals are valid only for $q \ll 1$ and hence, in general, are inapplicable to atoms in light.

In the present paper we address theoretically the problem of strong potentials. To simplify the discussion, we restrict our attention to time-stationary real potentials with a simple sinusioidal spatial profile (e.g., a standing off-resonance light wave for atoms). The analysis of time-dependent and complex potentials, for both small and large q, will be given elsewhere. To deal with the large-q values, we go beyond the two-beam ''dynamical'' diffraction long employed in neutron (and x-ray) diffraction [6–8] and reformulate the diffraction theory in terms of Mathieu functions [3,9,10]. The Mathieu function approach acknowledges the multiple-beam nature of diffraction right from the beginning and permits a systematic treatment of the problem for arbitrary power of the light beam.

The paper is organized as follows. In Sec. II we review, as background, the small-q wave functions long employed in dynamical diffraction theory. In Sec. III we show that separation of the two-dimensional Schrödinger equation for arbitrary q leads rigorously to a one-dimensional Mathieu equation and we note the physical meaning of the dimensionless parameters appearing in the Mathieu equation. In Sec. IV we

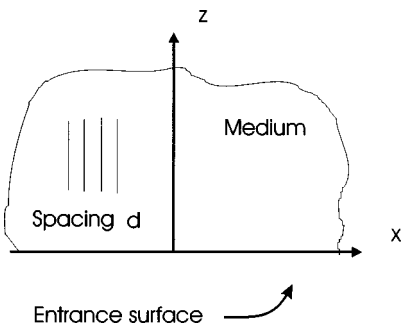

FIG. 1. Stage (the coordinates, the position of the medium, and the medium's entrance surface $z=0$) and orientation and spacing d of the planes of the periodic potential.

consider solutions known as Mathieu functions of integer order, note that physically these solutions apply when a particle is incident on the medium at a Bragg angle, and show that for small q these wave functions reduce to the well-known on-Bragg dynamical diffraction solutions. In Sec. V we present the wave functions for various q values and illumination conditions and note that the wave functions imply a rich generalization of the elementary pendellösung phenomena of dynamical diffraction theory. In Sec. VI we consider the asymptotic behavior of the solutions for large q, find that the wave functions become concentrated in the valleys of the medium, and note that, in this limit, the probability structure becomes, to some extent, independent of the incident angle (channeling). Section VII discusses some of the properties of the far field emerging from the medium after a certain depth is traversed by the wave. In Sec. VIII we describe the work still to be done on this topic: soft edges that admit adiabatic entry into the medium, off-Bragg illumination, imaginary and complex potentials, and time-dependent potentials.

Figure 1 sets the stage for the discussion. The plane $z=0$ is the entrance surface of the medium; the region $z<0$ has zero potential and the region $z>0$ is the periodic medium with a potential given by

$$V(x)=V_0+2V_1\cos Gx. \tag{2}$$

Here the x axis is along the entrance surface, $G\equiv 2\pi/d$, with d being the spacing of the potential peaks, and V_0 and V_1 are constants. Thus the surfaces of constant potential are planes perpendicular to both the plane of the figure and the entrance surface, i.e., a situation called the Laue case in crystal diffraction. In addition to satisfying Schrödinger's equation within the potential of Eq. (2), the wave function we seek must also satisfy boundary conditions at the entrance surface. We will assume that the incident particle has mass m and energy E and that the incident wave function is simply a plane wave whose wave vector has magnitude k, lies on the x-z plane, and has a negative-x component at or very close to $-G/2$. The z component of the incident wave vector is then

$$k_z=\left[k^2-\left(\frac{G}{2}\right)^2\right]^{1/2}. \tag{3}$$

In short, the plane-wave illumination in Fig. 1 is from the lower right at the Bragg angle.

Since V_0 and V_1 are zero for $z<0$ and constant for $z>0$, the medium has an abrupt or sharp edge. To describe a gentle or soft-edged medium one would have to let V_0 and V_1 be functions of z. We will not consider soft edges here. Also note that for atoms in standing light (built by an ideal single wave), we have from Eq. (1)

$$V_0=2V_1. \tag{4}$$

II. BACKGROUND

As background for the large-q wave functions, let us recall the two small-q wave functions Ψ^+ and Ψ^- used as base states in dynamical diffraction. These each have the factored form

$$\Psi^{\pm}(x,z,t)=\psi^{\pm}(x)e^{iK_z^{\pm}z}e^{-iEt/\hbar}, \tag{5}$$

but, as indicated, their x-axis wave functions $\psi^+(x)$ and $\psi^-(x)$ and their z-axis wave numbers K_z^+ and K_z^- are distinct. Specifically, the states, normalized over one potential period d, are

$$\psi^{\pm}(x)=\left(\frac{G}{4\pi}\right)^{1/2}(e^{iGx/2}\pm e^{-iGx/2}) \tag{6}$$

and their z-axis wave numbers are

$$K_z^{\pm}\equiv\left[k^2-\left(\frac{2m}{\hbar^2}\right)(V_0\pm V_1)-\left(\frac{G}{2}\right)^2\right]^{1/2}. \tag{7}$$

Note that for positive V_0 and V_1 and for $V_1<V_0$ both K_z^+ and K_z^- are less than the incident k_z given by Eq. (3), i.e., the particle must lose z momentum climbing into the positive-potential medium. Note also that while the $\psi^{\pm}(x)$ wave functions are each an equal-weight superposition of left- and right-running Bragg waves, $\psi^+(x)$ is a cosine with maximum probability for the particle to be at the peaks of the potential (2) and $\psi^-(x)$ is a sine with maximum probability at the valleys of the potential. Consequently, $\psi^+(x)$ experiences more potential than $\psi^-(x)$, which explains why $\psi^+(x)$ is associated with a smaller value of K_z than is $\psi^-(x)$. In fact, it has been noted [8] that the values K_z^+ and K_z^- given in Eq. (7) can be derived from the general energy constraint

$$K_z^{\pm}=\left[k^2-\left(\frac{2m}{\hbar^2}\right)\langle V\rangle^{\pm}-\left(\frac{G}{2}\right)^2\right]^{1/2}, \tag{8}$$

where $\langle V\rangle^{\pm}$ is the expectation value of the potential (2) for the state $\psi^{\pm}(x)$.

The two complete base states $\Psi(x,z,t)$ of Eq. (6) are a sufficient basis to match at the boundary $z=0$ any perfect Bragg illumination of the medium. By perfect Bragg illumination of the medium we mean a plane wave with k_x either $+G/2$ or $-G/2$ or an arbitrary superposition of both of these waves. For example, if the illumination is the single Bragg plane wave mentioned above, which approaches the entrance surface from the lower right in Fig. 1 with x momentum $-\hbar G/2$, then the resulting wave function in the medium is

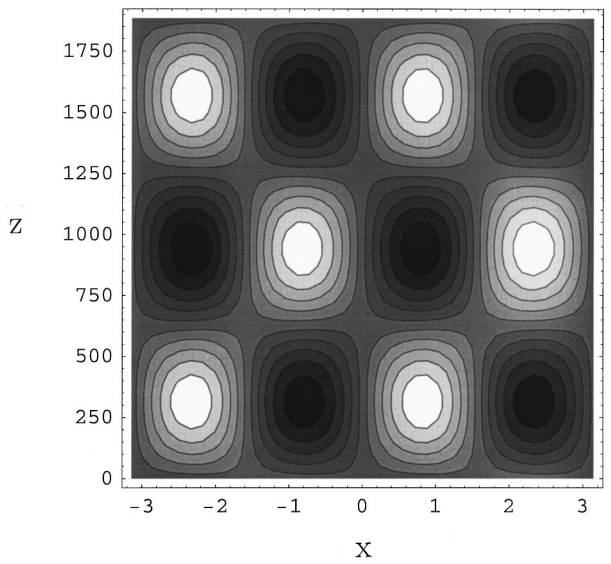

FIG. 2. Probability density plot $|\Psi(x,z)|^2$ of the in-medium field for $q=0.1$. The horizontal axis covers two potential periods with potential hills located in the center and on the edges. The vertical axis is the depth z. The white (black) areas indicate a significant increase (decrease) of the initial constant probability distribution, while the thin gray areas indicate as almost constant probability.

$$\Psi_{\text{total}}(x,z,t)=\frac{1}{\sqrt{2}}[\Psi^{+}(x,z,t)-\Psi^{-}(x,z,t)], \tag{9}$$

the minus sign removing the unwanted right-going waves at $z=0$ and thereby matching the incident left-going wave. Because of the different values of K_z^+ and K_z^-, a beating effect occurs with increasing depth z in the medium so that, even though the particle definitely had negative-x momentum at $z=0$, it will definitely have positive-x momentum at a depth $\Delta/2$, where

$$\Delta\equiv 2\pi(K_z^- - K_z^+)^{-1}, \tag{10}$$

and will return to negative-x motion at Δ, etc. The depth Δ is known as the pendellösung length and the oscillations of the direction of propagation are known as pendellösung oscillations. Figure 2 shows the probability distribution $|\Psi_{\text{total}}(x,z,t)|^2$ of the total state over two potential periods in the x direction, i.e., there is a potential peak at the center of the horizontal axis and one at each edge of the figure and over $1\frac{1}{2}$ pendellösung depths Δ in the z direction ($\Delta=1250$ of the arbitrary vertical units). As the particle enters at $z=0$ going left, the intensity is uniform across the entrance surface. In the medium the amplitude splits into two waves having different wave numbers (see Fig. 3). Due to their mutual beating, the probability density piles up on the left-hand side of each channel at $z=\Delta/4$ and then it is uniform again at depth $\Delta/2$. However, now the particle is propagating to the upper right, i.e., it has been turned by Bragg diffraction. The states ψ^+ and ψ^- are called, respectively, ψ^β and ψ^α by x-ray crystal diffractionists and ψ_2 and ψ_1 by neutron crystal diffractionists.

The base states $\Psi^\pm$ out of which the total state of Eq. (9) is constructed are not exact solutions of Schrödinger's equation in the potential (2), but as we shall see they are approximate solutions when the potential V_1 is small compared to the x-axis kinetic energy $\hbar^2(G/2)^2/2m$ of a particle obeying the first-order Bragg condition. For use below let us introduce the dimensionless ratio of these energies as the parameter q,

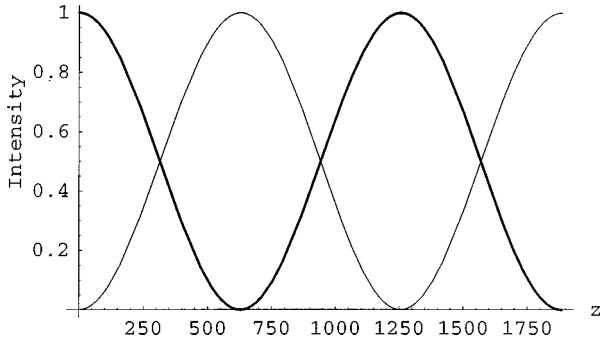

FIG. 3. Depth dependence of the intensity for the left going (thick line) and right going (thin line) waves. The two intensities are sinusoidal and mutually out of phase by π.

$$q\equiv\frac{8mV_1}{\hbar^2G^2}. \tag{11}$$

III. FROM SCHRÖDINGER TO MATHIEU

To find the base wave functions for large q, consider the two-dimensional Schrödinger equation in the potential (2),

$$i\hbar\frac{\partial\Psi}{\partial t}+\frac{\hbar^2}{2m}\nabla^2\Psi-V_0\Psi-2V_1\cos(Gx)\Psi=0. \tag{12}$$

We seek factored base states just as in Eq. (5), i.e.,

$$\Psi(x,z,t)=\psi(x)e^{iK_zz}e^{-iEt/\hbar}, \tag{13}$$

except that for large q, $\psi(x)$ and K_z are no longer given by Eqs. (6) and (7) and, as we shall see, in general, more than two base states will be needed at large q. Insertion of Eq. (13) into Eq. (12) and introduction of a dimensionless coordinate $Gx/2\rightarrow x$ leads to the equation

$$\frac{d^2\psi}{dx^2}+[a-2q\cos(2x)]\psi=0 \tag{14}$$

for the x-axis wave function, where the new dimensionless parameter a is defined as

$$a\equiv\frac{4}{G^2}\left[\left(\frac{2m}{\hbar^2}\right)(E-V_0)-K_z^2\right]. \tag{15}$$

Equation (14) is the standard form of the Mathieu equation and its solutions are known as Mathieu functions.

In Sec. IV we consider integer-order Mathieu functions since they are the base states needed to develop wave functions generated by perfect Bragg illumination. They deliver a sufficient set of functions so that at the entrance we can perfectly match any incoming Bragg illumination. Before considering these functions let us first emphasize the wave-

mechanical significance of the Mathieu parameter a. Consider a periodic Schrödinger probability amplitude ψ that obeys the Mathieu equation. Multiply Eq. (14) by ψ^* and integrate over whatever period has been chosen for normalization, say, π. (Note that in the dimensionless coordinate, the period of the potential is π; the base state functions in Sec. IV are all periodic over either π or 2π, but their squares are periodic over π, like the potential.) Use the normalization and solve for a to obtain

$$a = 2q\int_0^{\pi} \psi^* \cos(2x)\,\psi\,dx - \int_0^{\pi} \psi^* \frac{d^2\psi}{dx^2}\,dx. \qquad (16)$$

The first term is the expectation value of the sinusoidal part of the potential and the second term (including the minus sign) is the expectation value of the kinetic energy in the x direction, both terms in a dimensionless format. Equation (16) implies that any specific ψ that obeys Eq. (14) must be accompanied by a specific or characteristic value of the parameter a. Since K_z is the only free parameter in Eq. (15) defining a (G, E, and V_0 are assumed given and fixed), each specific solution will be associated with a specific value of K_z. In short, the detailed shape of an x-axis base state will fix the associated z-axis momentum, the same behavior seen earlier in Eq. (8) for the small-q base states. Equating Eqs. (15) and (16) and solving for K_z, one obtains the generalization of Eq. (8) for base states of arbitrary q.

Two comments are in order about this section. First, it should be noted that the argument given here, from the Schrödinger equation (12) through Eqs. (15) and (16) to a generalization of Eq. (8), constitutes a rigorous derivation of a previous conjecture [8] that the longitudinal wave number is determined by the transverse wave function via energy expectation values. However, the current argument does not immediately yield a related conjecture [8] that the correct transverse wave function yields an extremum for the potential-energy expectation value. Second, curiously enough for large E and $q \approx 1$, the pendellössung length is of the order of the Talbot distance [11].

IV. MATHIEU FUNCTIONS OF INTEGER ORDER

For each integer $n \geqslant 0$ their exist two integer-order Mathieu functions: one even in x denoted $\mathrm{ce}_n(x,q)$ and one odd in x denoted $\mathrm{se}_n(x,q)$. Each is real and has period π or 2π. The even [odd] one $\mathrm{ce}_n(x,q)$ [$\mathrm{se}_n(x,q)$] can be expanded as a Fourier cosine [sine] expansion with real coefficients and with the lead term being $\cos(nx)$[$\sin(nx)$]. There is also a zeroth-order Mathieu function $\mathrm{ce}_0(x,q)$ that is even and periodic and has a lead Fourier term of a constant followed by $\cos(2x)$. In all the Fourier expansions of the integer Mathieu functions only alternate terms appear [9]:

$$\mathrm{ce}_{2n}(x,q) = \sum_{r=0}^{\infty} A_{2r}^{(2n)}(q)\cos(2rx) \quad [a_{2n}(q)], \qquad (17)$$

$$\mathrm{se}_{2n+1}(x,q) = \sum_{r=0}^{\infty} B_{2r+1}^{(2n+1)}(q)\sin[(2r+1)x] \quad [b_{2n+1}(q)], \qquad (18)$$

$$\mathrm{ce}_{2n+1}(x,q) = \sum_{r=0}^{\infty} A_{2r+1}^{(2n+1)}(q)\cos[(2r+1)x] \quad [a_{2n+1}(q)], \qquad (19)$$

$$\mathrm{se}_{2n+2}(x,q) = \sum_{r=0}^{\infty} B_{2r+2}^{(2n+2)}(q)\sin[(2r+2)x] \quad [b_{2n+2}(q)]. \qquad (20)$$

As anticipated in Sec. III, each integer-order Mathieu function is a solution of the Mathieu equation (14) only if the parameter a has the appropriate characteristic value. The standard notation for these values is shown in the square brackets next to the Fourier expansion of each function (17)–(20). As indicated, both the expansion coefficients and the characteristic values are q dependent.

For sufficiently small q the Fourier coefficients can be expressed as power series in q. For $\mathrm{ce}_1(x,q)$ and $\mathrm{se}_1(x,q)$ one finds [9]

$$\mathrm{ce}_1(x,q) = \cos x - \frac{q}{8}\cos 3x + q^2 \times\left[\tfrac{1}{192}\cos 5x - \tfrac{1}{64}\cos 3x - \tfrac{1}{128}\cos x\right] + O(q^3), \qquad (21)$$

$$\mathrm{se}_1(x,q) = \sin x - \frac{q}{8}\sin 3x + q^2 \times\left[\tfrac{1}{192}\sin 5x + \tfrac{1}{64}\sin 3x - \tfrac{1}{128}\sin x\right] + O(q^3). \qquad (22)$$

To zeroth order in q, $\mathrm{ce}_1(x,q)$ is $\cos x$ and $\mathrm{se}_1(x)$ is $\sin x$ and hence we recover the dynamical diffraction base state $\psi^{\pm}(x)$ of Eq. (6), but here unnormalized.

For sufficiently small q the characteristic constants can be expressed as power series of q. For $\mathrm{ce}_1(x,q)$ and $\mathrm{se}_1(q,x)$ these are, respectively [9],

$$a_1(q) = 1 + q - \frac{q^2}{8} - \frac{q^3}{64} + \cdots, \qquad (23)$$

$$b_1(q) = 1 - q - \frac{q^2}{8} + \frac{q^3}{64} + \cdots. \qquad (24)$$

To first order in q, when Eq. (15) for a and Eq. (11) for q are inserted into Eq. (23), the expression of Eq. (7) for K_z^+ is recovered. Similarly, Eq. (24) to first order in q yields the value of K_z^-. Thus the complete dynamical diffraction theory is contained in two Mathieu functions to zeroth order in q and in their characteristic values to first order in q.

For large q neither the expansion coefficients nor the characteristic values can be determined from such power series and so one has to resort to standard numerical techniques [9], which we will do shortly. These numerical techniques adopt the normalization for the Mathieu functions

$$\frac{1}{\pi}\int_0^{2\pi} \mathrm{ce}_n^2(q,x) = \frac{1}{\pi}\int_0^{2\pi} \mathrm{se}_n^2(q,x) = 1. \qquad (25)$$

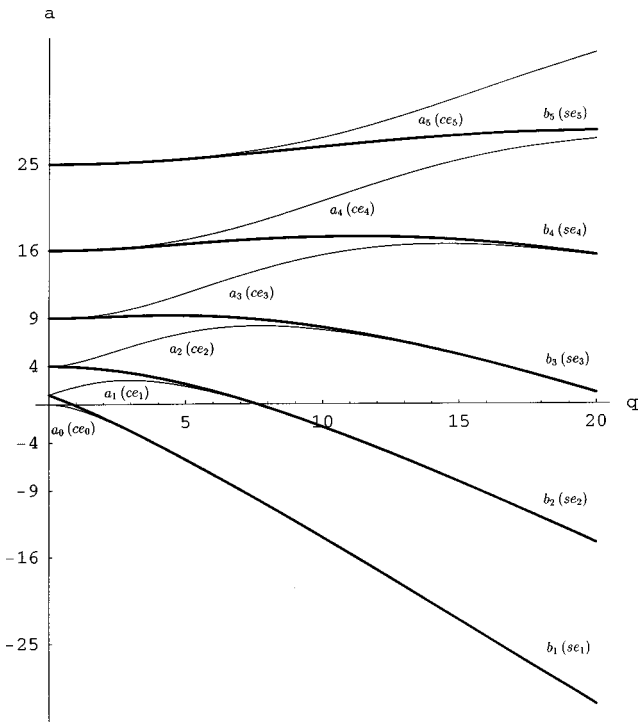

FIG. 4. Characteristic values for the lowest-order Mathieu functions as a function of q.

The normalization condition can be rewritten using the expansion coefficients as

$$2[A_0^{(2n)}]^2+\sum_{r=1}^{\infty}[A_{2r}^{(2n)}]^2=1, \tag{26}$$

$$\sum_{r=0}^{\infty}[B_{2r+1}^{(2n+1)}]^2=\sum_{r=0}^{\infty}[A_{2r+1}^{(2n+1)}]^2=\sum_{r=0}^{\infty}[B_{2r+2}^{(2n+2)}]^2=1. \tag{27}$$

The factor 2 for the lead coefficient in the ce_{2n} Mathieu functions comes from the constant term that is present in those expansions. Because of this the lowest Mathieu function $\mathrm{ce}_0(q,x)$ is positive everywhere. It is important to note that the Mathieu functions for a given q are orthogonal:

$$\int_0^{2\pi}\mathrm{se}_m(q,x)\mathrm{ce}_n(q,x)=0, \tag{28}$$

$$\frac{1}{\pi}\int_0^{2\pi}\mathrm{se}_m(q,x)\mathrm{se}_n(q,x)=\frac{1}{\pi}\int_0^{2\pi}\mathrm{ce}_m(q,x)\mathrm{ce}_n(q,x)=\delta_{mn}. \tag{29}$$

The techniques for calculating both the expansion coefficients and the characteristic values at arbitrary q are described in detail in [9] and are now available on commercial mathematical software. Figure 4 shows the characteristic values associated with the lowest-order Mathieu functions as a function of q. Figures 5 and 6 show the lowest-order functions over two potential periods and for various q values. Several features deserve comments. First, at zero q the characteristic value for both the spatially even and spatially odd functions of order n is n^2. This is because, with no potential, the characteristic value is just the x-axis kinetic energy and, since only the lead term in the functions, i.e., $\cos(nx)$ or $\sin(nx)$, is present at $q=0$, the (dimensionless) kinetic energy is simply n^2. Second, with increasing q the characteristic value for the spatially odd function stays below that for the spatially even function of the same order. This is because the spatially even function ''sees'' the potential more.

Third, with q sufficiently in excess of 1, the characteristic values of ce_0 and se_1 (and ce_1 and se_2, etc.) asymptotically converge, indicating that these two functions tend toward the same energy expectation value. Since for large q the potential energy dominates the kinetic, the convergence of these characteristic values actually indicates that the two functions have the same expectation value for the potential, i.e., the squares of the functions must have the same shape. The graphs of ce_0 and se_1 at $q=24$ confirm this and a similar convergence can be seen in the pairs of functions in Fig. 6. Note that for the higher-order pairs the convergence does not fully develop until larger-q values are achieved because of their greater kinetic energy.

Fourth, while the functions of even order $n=0,2,4,...$ have period π and those of odd order $n=1,3,5,...$ have period 2π, the squares of all the functions have period π, the same as the potential. Fifth, for all the functions there is a general tendency, with increasing q, for the probability density to be pushed off the potential peaks and into the valleys, i.e., coherent quantum-mechanical channeling. To see this in the graphs, it is important to remember that the period of the potential is π, in the dimensionless coordinate, and thus the domain of the graphs is two periods of the potential, i.e., there is a potential peak at the center and at each edge of the graph. Finally, as the probability density gets more localized in the valleys with increasing q, higher-order components are required in the Fourier expansions of the functions.

V. TOTAL WAVE FUNCTION

The Mathieu functions of integer order will now be used to develop the total wave function $\Psi(x,z)$ produced in a medium of arbitrary q by an atom incident under Bragg conditions. Under Bragg conditions this function Ψ at the entrance surface will have the same period π as the potential. For a given q the corresponding integer-order Mathieu functions are mutually orthogonal and form a complete set for expanding any function that shares the periodicity of the medium. Thus the incident function can be decomposed

$$\Psi(x,0)=\sum_n[c_n\mathrm{ce}_n(q,x)+d_n\mathrm{se}_n(q,x)], \tag{30}$$

where the expansion coefficients are

$$c_n=\frac{1}{\pi}\int_0^{2\pi}\mathrm{ce}_n(q,x)\Psi(x,0)dx, \tag{31}$$

$$d_n=\frac{1}{\pi}\int_0^{2\pi}\mathrm{se}_n(q,x)\Psi(x,0)dx. \tag{32}$$

Since each Mathieu function is linked to a specific characteristic constant $a_n[b_n]$ and hence, via Eq. (15), to a specific wave number K_z, the complete in-medium function $\Psi(x,z)$

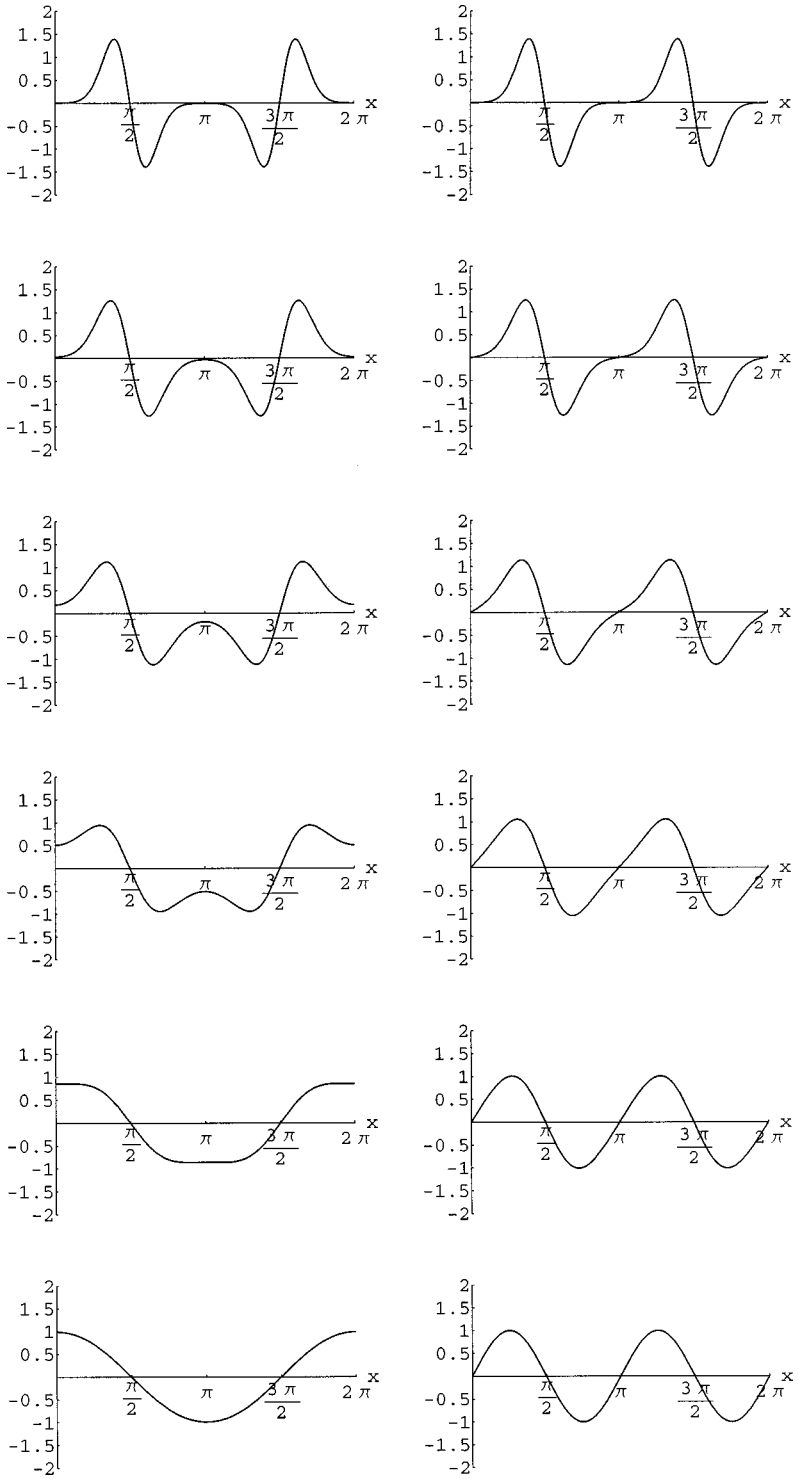

FIG. 5. Mathieu functions ce_0 (left) and se_1 (right) over two periods of the potential and $q=0.1$, 1, 3, 6, 12, 24, with q increasing from bottom to top. Note that a potential hill is on each of the edges and in the center.

is obtained by multiplying each Mathieu function by the appropriate z-dependent exponential. Thus the total wave function in the medium is

$$\Psi(x,z)=\sum_{n=0}^{\infty} c_n \mathrm{ce}_n(q,x)\exp(iK_1^n z) + \sum_{n=0}^{\infty} d_n \mathrm{se}_n(q,x)\exp(iK_2^n z), \tag{33}$$

where from Eq. (15)

$$K_1^n=\sqrt{\frac{2m}{\hbar^2}(E-V_0)-\frac{G^2}{4}a_n(q)}, \tag{34}$$

$$K_2^n=\sqrt{\frac{2m}{\hbar^2}(E-V_0)-\frac{G^2}{4}b_n(q)}. \tag{35}$$

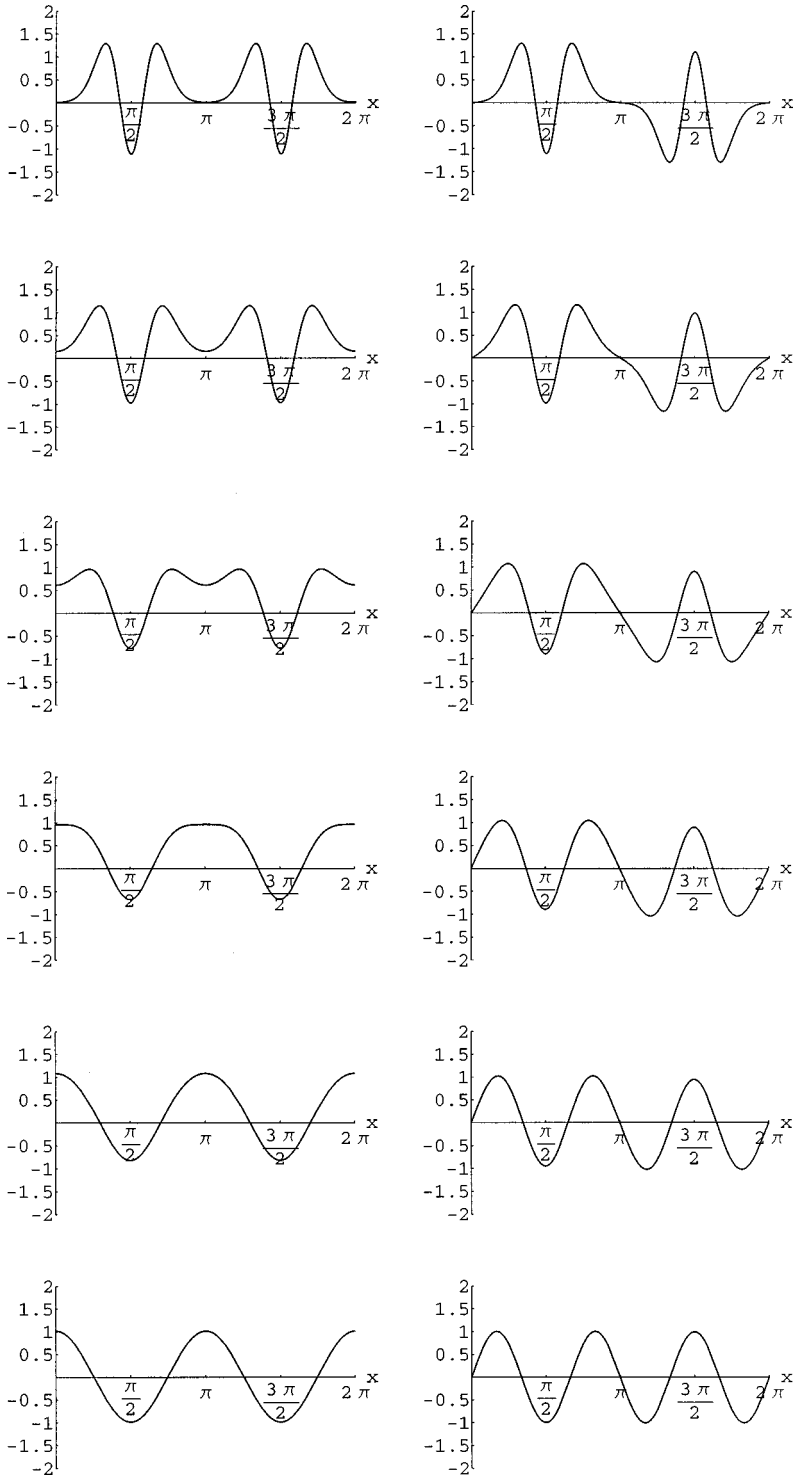

FIG. 6. Mathieu functions ce_1 (left) and se_2 (right) over two periods of the potential and $q=0.1$, 1, 3, 6, 12, 24, with q increasing from bottom to top. Note that a potential hill is on each of the edges and in the center.

Note that, although each term factors into functions of x and z, the complete wave function does not factor, just as in the small-q solution (9). To prepare a factorizable in-medium wave function, i.e., a single Mathieu function times a single z-axis exponential, one would need to illuminate the entrance surface with a coherent superposition of plane waves $\exp(\pm ix)$, $\exp(\pm 2ix)$, $\exp(\pm 3ix)$,..., with appropriate amplitudes and phases.

Consider as the first example the left-going and perfect Bragg incident wave discussed in Secs. I and II. The wave's x dependence in the dimensionless coordinate is simply

$$\Psi(x,0)=\exp(-ix)=\cos x-i\sin x. \tag{36}$$

Figure 7 displays, for increasing-q values, the probability density $\Psi(x,z)$ of the in-medium wave function (33) for this illumination. The given plots call for several comments. First, for small q the typical pattern of Bragg diffraction can

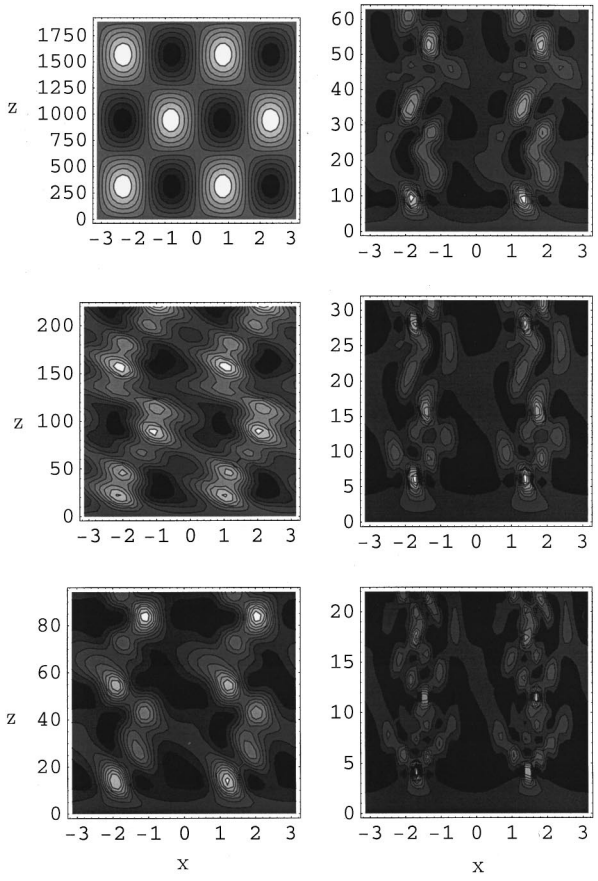

FIG. 7. In-medium density plots for left-going Bragg illumination and increasing q. The plots are paired from top to bottom $q=\{0.1,6\}$, $\{1, 12\}$, and $\{3, 24\}$.

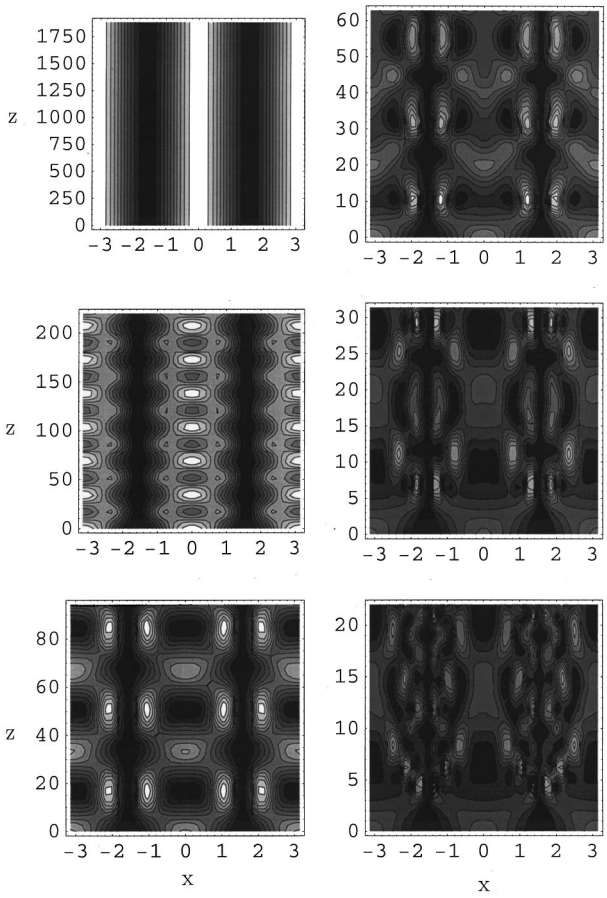

FIG. 8. In-medium density plots for cosine illumination for increasing q. The plots are paired from top to bottom $q=\{0.1,6\}$, $\{1, 12\}$, and $\{3, 24\}$.

be seen. When q increases the frequencies of the oscillation become larger, i.e., the pendellösung length becomes shorter (note the change in the z scale). Second, the probability density becomes more modulated due to the appearance of additional frequencies. This is due to the excitation of additional in-medium states [apart form the lowest $\mathrm{ce}_1(q,x)$ and $\mathrm{se}_1(q,x)$]. Formally speaking, the overlap between the incident wave and the lowest state is not sufficient to guarantee satisfaction of the boundary condition at the entrance surface. Third, the plots become more localized in the valley. This is a direct consequence to the properties of the in-medium states discussed in Sec. IV. Fourth, in the case of large q the distribution becomes almost symmetrical along the x axis about the minimum of the potential. The initial asymmetric illumination is remembered only as a slight zigzag motion in the valley.

As a second example consider two-wave illumination. If the two waves have zero phase at the potential peaks this gives

$$\Psi(x,0)=\tfrac{1}{2}[\exp(ix)+\exp(-ix)]=\cos x. \tag{37}$$

However, if the two waves are in phase at the potential valleys then the incident field is

$$\Psi(x,0)=\frac{1}{2i}[\exp(ix)-\exp(-ix)]=\sin x. \tag{38}$$

Such standing wave states have actually been produced at the third grating of existing interferometers [12]. Figure 8 shows, for increasing q, the in-medium probability density for the cosine illumination. Similarly, Fig. 9 displays the probability density for sine illumination. In both cases we deal with symmetric initial conditions (of the initial probability density) with respect to the z axes (at the point $x=0$). This symmetry is preserved for all the in-medium density plots irrespective of q. In the small-q case both incident waves excite only one of the in-medium states and we expect no modulation of the probability density as the wave penetrates the medium, i.e., no pendellösung behavior. With an increase of q the scales in z change, i.e., the frequencies increase again.

For the incident cosine wave the probability density is pushed off the potential hills into the valleys as q increases. There is, however, always a zero probability line along the center of the valley due to the structure of the odd cosinelike Mathieu functions. For large q the probability is concentrated in peaks. We will focus on this effect in Sec. VI.

From the beginning the incident sine wave is already quite localized in the valleys and hence the modulation with increasing q does not go through such a dramatic change as the cosine wave. Formally, this is to be explained by the overlap with the in-medium states. The spread over in-medium states for a sine wave is weaker than for the cosine wave and hence a less spectacular modulation has to be expected.

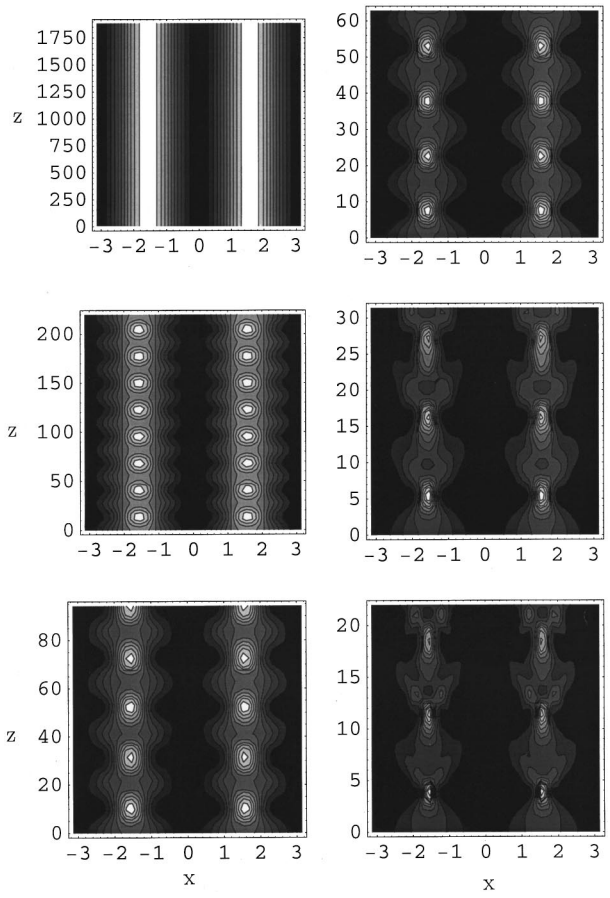

FIG. 9. In-medium density plots for sine illumination for increasing q. The plots are paired from top to bottom $q=\{0.1, 6\},\{1, 12\}$, and $\{3, 24\}$.

Finally, as the last example, consider a single plane-wave incident normal to the entrance face of the medium. Then the unnormalized incident x function is

$$\Psi(x,0)=\text{const.} \tag{39}$$

Figure 10 shows, for increasing q, the in-medium probability density. As in the previous case, the in-medium probability density is strictly symmetric about the center of the valley. Even though the incident wave is spread evenly over the whole period of the potential, with increasing q, the probability in the medium is again focused into the valley. A further increase in q leads to additional structures, which will be considered in the next section.

VI. LARGE-q LIMIT

In Sec. IV we pointed out that, for large q, adjacent cosinelike and sinelike base states acquire the same shape (up to a sign); that this shared shape has a distinctive number of peaks (dependent on the order of the function), and that the peaks are located in the valley of the potential (channeling). In addition, as the functions converge in shape with increasing shape, their characteristic constants and hence their associated K_z wave numbers also converge. As a consequence of these convergences, some regularities in the in-medium probability densities should develop. Figure 11 shows the densities at $q=50$ for the four previously considered illumi-

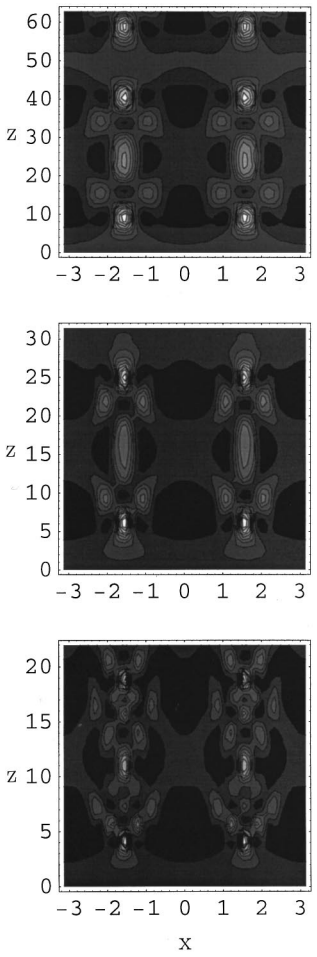

FIG. 10. In-medium density plots for normal illumination for increasing q, with $q=6$, 12, 24 from top to bottom.

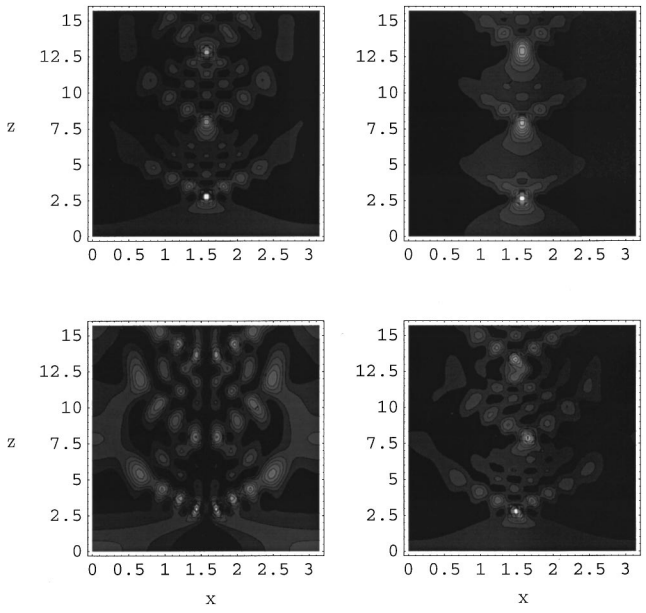

FIG. 11. In-medium density plots for the high-q regime ($q=50$). The plots are paired from top (normal, sine illumination) to bottom (cosine, left-going Bragg illumination), and each spans only one period of the potential.

TABLE I. Expansion coefficient for normal incidence and $q=50$.

n	c_n
0	0.5542
1	0.4136
2	0.3859
3	0.3993
4	0.4244
5	0.1811
6	0.0200

nations. Along the bottom of each valley, there is a sequence of dominant peaks equally spaced in depth and these peaks are interconnected via a net of additional but less pronounced concentrations of probability. One might attempt to understand some of these patterns via classical mechanics. However, in this section we will give the simple wave mechanics behind these patterns.

Let us choose as an example the normal incidence illumination. For normal incidence the wave function can be written as the sum of only even, i.e., ce_{2n}, Mathieu functions and hence the probability density as

$$|\Psi(x,z)|^2=\left|\sum_{n=0}^{\infty} c_{2n}\mathrm{ce}_{2n}(q,x)\exp(iK_1^{2n}z)\right|^2. \quad (40)$$

This equation can be rewritten as

$$|\Psi(x,z)|^2=\sum_{n=0}^{\infty} c_{2n}^2\mathrm{ce}_{2n}^2(q,x) + 2\sum_{n=0}^{\infty} c_{2n}c_{2m}\mathrm{ce}_{2m}(q,x)\mathrm{ce}_{2n}(q,x) \times\cos[(K_1^{2n}-K_1^{2m})z] \quad (41)$$

or

$$|\Psi(x,z)|^2=F(x)+2\sum_{n=0}^{\infty} c_{2n}c_{2m}\mathrm{ce}_{2m}(q,x)\mathrm{ce}_{2n}(q,x) \times\cos[(K_1^{2n}-K_1^{2m})z], \quad (42)$$

where the z-independent part was summed into the function $F(x)$. For $q=50$, the expansion coefficients c_{2n} are given in Table I for reference. To understand the structure of the probability distribution as shown in Fig. 11 we first look at the form of the Mathieu functions for large q. In Sec. IV [Eqs. (21) and (22)] we gave the unnormalized expansion for the lowest Mathieu functions. In general, the leading terms are always $\cos(nx)$ and $\sin(nx)$ (n is the order of the Mathieu function) and the size of the remainder depends on the value of q and n. When q increases the lower-order functions depart significantly from the cosinelike or sinelike behavior. In Fig. 12 we show the first eight even-order ce_{2n} Mathieu functions for $q=50$. The lower-order functions are nonzero only in the middle of the plotted interval, i.e., in the region corresponding to the valley of the medium. The higher-order Mathieu functions still do not depart dramatically from the cosine shape. However, for a given q the high-order functions are not needed as their overlap with the incident wave is negligible; we find that about $\sqrt{q}$ Mathieu functions are needed to match the incident wave. The function $F(x)$ is a weighted sum of the squared Mathieu functions and is shown in Fig. 13 for all the mentioned illuminations. The functions $F(x)$ can be understood as the complete probability density averaged over large z. For normal incidence it shows a central peak and symmetrically spaced side peaks coming from the higher-order Mathieu functions. The complete pattern of $|\Psi(x,z)|^2$ comes from the additional z-dependent sum in Eq. (42). At the entrance ($z=0$) the probability distribution is constant and equals one. As we proceed into the medium the

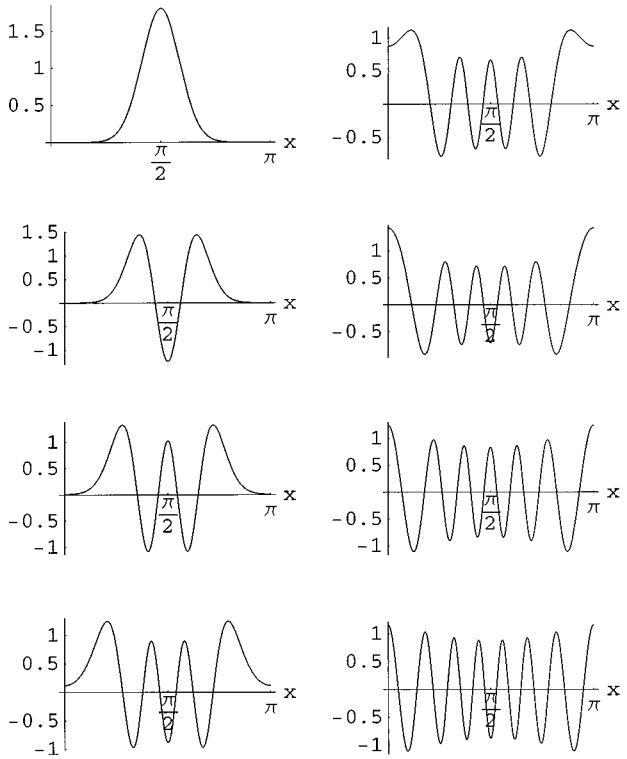

FIG. 12. Mathieu functions ce_{2n} $n=0-7$ over one period of the potential and $q=50$. The value n increases from top to bottom and from left to right. Note that a potential hill is at each of the edges and a valley is in the center.

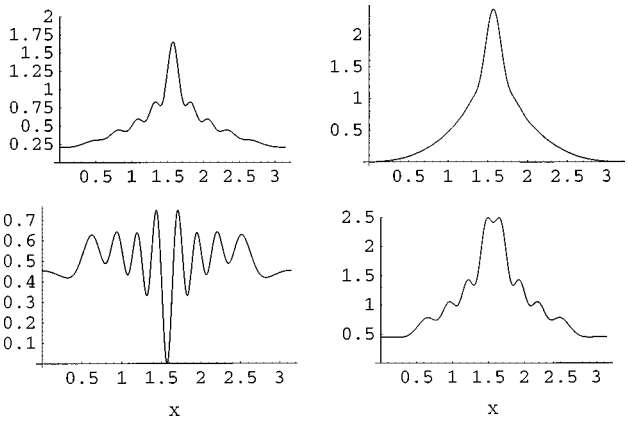

FIG. 13. Plots of the function $F(x)$ for the four illuminations considered in Fig. 11.

distribution is modulated. The modulation is controlled by the phases defined by the product of the depth z and the wave-number differences $K_1^{2m}-K_1^{2n}$.

For large q the characteristic constants $a_n(q), b_n(q)$ can be approximated as [9]

$$a_{2n}(q)\approx -2q+(8n+2)\sqrt{q}, \tag{43}$$

$$a_{2n+1}(q)\approx -2q+(8n+6)\sqrt{q}, \tag{44}$$

$$b_{2n+1}(q)\approx -2q+(8n+2)\sqrt{q}, \tag{45}$$

$$b_{2n+2}(q)\approx -2q+(8n+6)\sqrt{q}. \tag{46}$$

From these relations we infer that the distance between the lowest levels becomes an integer multiple of the basic distance $8\sqrt{q}$,

$$a_{2m}(q)-a_{2n}(q)\approx (m-n)8\sqrt{q}. \tag{47}$$

In our present case the basic frequency is associated with the difference $K_1^0-K_1^2$ as determined by the lowest characteristic values a_0 and a_2 (which are both negative for large q). Therefore, the first significant change should come at a depth z, where

$$(K_1^0-K_1^2)z=\pi, \tag{48}$$

which can be rewritten in the form

$$z=\frac{8\pi\sqrt{E}}{a_2(q)-a_0(q)}\,\frac{\sqrt{2m}}{\hbar G^2}. \tag{49}$$

At this depth the significant terms to be added to $F(x)$ are $(n\geqslant 0)$

$$-c_{2n}c_{2n+2}\mathrm{ce}_{2n}(x,q)\mathrm{ce}_{2n+2}(x,q). \tag{50}$$

These pairs of functions $\mathrm{ce}_{2n}, \mathrm{ce}_{2n+2}$ have a peak at $\pi/2$ but with opposite sign, so they add to the central peak of $F(x)$ as we have a minus sign in front of the term coming from the phase. The side peaks come with the same sign and have to be subtracted from the function $F(x)$. In addition to these terms, we must add the combinations

$$c_{2n}c_{2n+4}\mathrm{ce}_{2n}(x,q)\mathrm{ce}_{2n+4}(x,q), \tag{51}$$

as they have an accumulated phase of 2π. Other terms can be neglected due to the small value of their expansion coefficients. As a consequence of the periodicity, we expect another dominant peak after an additional accumulated 2π shift. In this way we are able to explain the appearance of the dominant peaks and their periodicity.

The next significant phase change occurs at

$$(K_1^0-K_1^2)z=2\pi. \tag{52}$$

The central peaks of the Mathieu functions $\mathrm{ce}_0(x,q)$ and $\mathrm{ce}_2(x,q)$ have opposite signs and have to be subtracted from $F(x)$. The two side peaks of $\mathrm{ce}_2(x,q)$ have the same sign as $\mathrm{ce}_0(q,x)$ and are added to $F(x)$. Including also the other combinations of terms, we explain the line of four minor peaks between the two dominant peaks. The additional fine structure can be explained via similar arguments.

In this analysis we assumed that the differences of the separation constants are exactly commensurate. However, this assumption is only approximately valid; the wave numbers are definitely incommensurate and hence patterns will be smeared out as we go deeper. However, with an additional increase of q we should expect the appearance of additional peaks and also that the resolution of the peaks improves.

VII. OUTGOING PLANE-WAVE INTENSITIES

A directly measurable quantity in Bragg diffraction experiments is the relative intensity distribution of the various outgoing plane waves. After traversing a certain depth in the medium the various plane waves are released at the back exit surface and, due to their diverging momenta, the various plane waves will spatially separate at a sufficient distance from the exit surface. The probability of releasing the component $\exp(\pm inx)$ at a depth z in the medium is given by

$$P(n)=\tfrac{1}{4}\left|\sum_{m=0}^{\infty} c_m(q)A_n^{(m)}(q)\exp[iK_1^m(q)z] - \sum_{m=0}^{\infty} d_m(q)A_n^{(m)}(q)\exp[iK_2^m(q)z]\right|^2, \tag{53}$$

$$P(-n)=\tfrac{1}{4}\left|\sum_{m=0}^{\infty} c_m(q)A_n^{(m)}(q)\exp[iK_1^m(q)z] + \sum_{m=0}^{\infty} d_m(q)A_n^{(m)}(q)\exp[iK_2^m(q)z]\right|^2, \tag{54}$$

where $c_m(q)$ and $d_m(q)$ are coefficients defined by the boundary condition, i.e., the expansion coefficients in Eq. (30). $A_m^{(n)}(q), B_m^{(n)}(q)$ are the overlap coefficients between the base states and the exponentials $\exp(\pm inx)$, i.e., the fourier coefficients. For the probabilities the normalization condition holds

$$\sum_n^{\infty} [P(n)+P(-n)]=1. \tag{55}$$

The intensities of the components vary with changing q and increasing depth. We plot two samples for the component intensities in Fig. 14 and two more in Fig. 15. Figure 14 is for normal incidence and Fig. 15 is for the left-going plane wave impinging at a Bragg angle. In the case of normal incidence only one set $P(2n)$ is displayed due to the symmetry $P(2n)=P(-2n)$.

For very small q the normal incoming wave has a large overlap only with the zeroth-order base state function and hence the intensity $P(0)$ is almost unity at all depths. For increased q additional base states are excited and as a consequence additional diffraction orders appear. As a rule of thumb we have found that for a given q about $\sqrt{q}$ orders will be significantly excited. For high q we see an interesting behavior. The incoming zeroth-order component excites a sequence of peaks in the higher orders and is at a certain

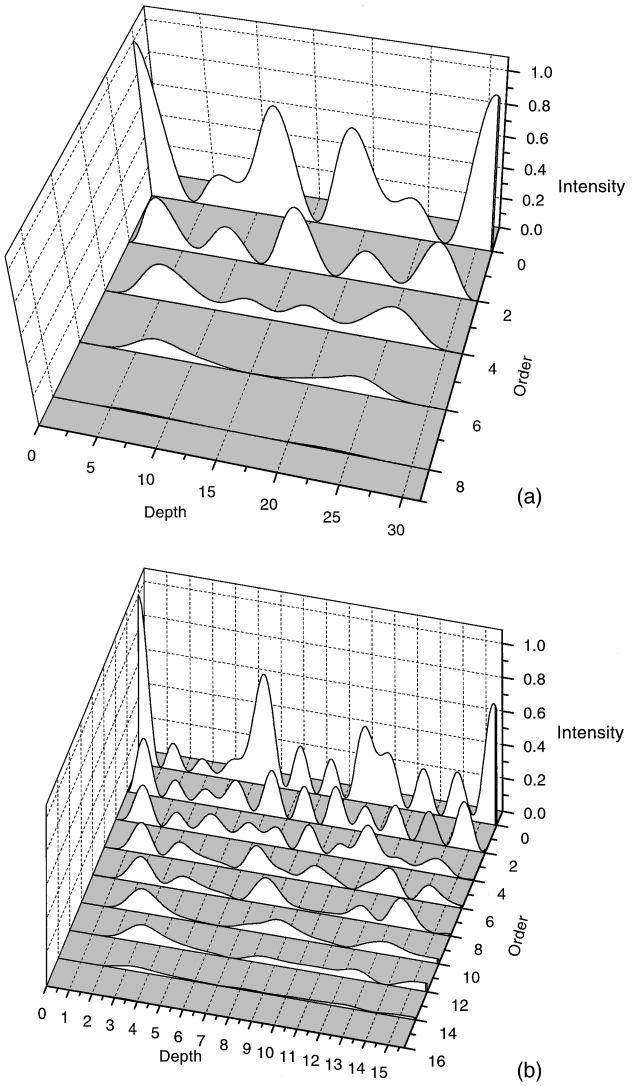

FIG. 14. (a) Intensities of $P(2n)$ for a normal incident wave and $q=12$. The corresponding in-medium probability density is given in the center plot of Fig. 10. Due to the symmetry of the diffraction orders, only the positive orders are displayed. Higher-order diffraction components oscillate less frequently. (b) Intensities of $P(2n)$ for a normal incident wave and $q=50$.

depth exhausted. However, at a greater depth it revives and then generates another sequence.

In the case of Bragg illumination and a small q the incoming wave excites only two in-medium base states: cosine and sine states associated with different wave numbers $K^1_{1,2}$. The outgoing plane-wave intensities then follow the equations

$$P(-1)=\tfrac{1}{2}\{1+\cos[(K^1_1-K^1_2)z]\} \tag{56}$$

and

$$P(1)=1-P(-1)=\tfrac{1}{2}\{1-\cos[(K^1_1-K^1_2)z]\}. \tag{57}$$

These two functions were shown above in Fig. 3. When q increases the total intensity spreads over several orders. Even though the structures become more involved, several typical features can be observed. First, with increasing order the maximum intensity decreases. Second, the higher orders become significantly different from zero always for a larger depth than the lower orders. Third, the first few oscillations of the initially excited order are copied (with a shift) by the higher-order terms. Fourth, the period of the oscillations of the higher-order intensities is longer than for the lower orders. This behavior can be understood by looking at the form of Eqs. (53) and (54).

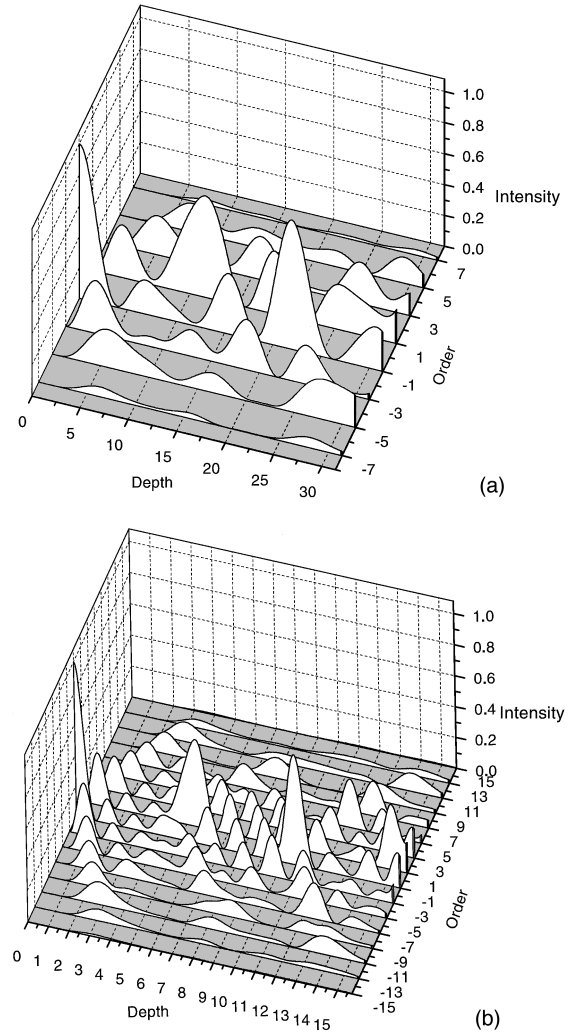

FIG. 15. (a) Intensities of $P(2n+1)$ for the on Bragg incident wave and $q=12$. The corresponding in-medium probability density is given in the right center plot of Fig. 7. The dominant peaks for the orders -1 and $+1$ are the remains of the original pendellösung from Fig. 2. (b) Intensities of $P(2n+1)$ for $q=50$.

Finally, we should mention also that for large q, symmetric pairs of higher-order waves (i.e., n and $-n$) start to oscillate in phase. This is in contrast with the lowest pairs of symmetric waves, which oscillate with a phase shift of $\pi/2$ (recall Fig. 3).

VIII. CONCLUSIONS

The base states introduced in Sec. IV and the total wave functions found in Sec. V solve the problem posed in the Introduction: Find the Schrödinger wave function generated in a medium with strong sinusoidal potential when the medium has a sharp boundary and is illuminated by a perfect Bragg plane wave or normally incident wave of definite

energy. The wave functions are built by superposition of products of integer-order Mathieu functions in x and complex exponentials in z with wave numbers characteristic of each Mathieu function. Each term in the superposition is a rigorous solution of the Schrödinger equation in the periodic medium and the superpositions rigorously match the incident plane wave at the boundary. When the potential is weak the wave functions reduce to the familiar perfect Bragg wave functions of dynamical diffraction theory. Using these functions we are able to predict the behavior of the matter wave in the medium and the intensities of the various plane waves released after depth z in the medium.

Several extensions are called for. First, in current experiments with atoms impinging on standing light, the incident radiation is not a single perfect Bragg plane wave but typically is a mixture of many plane waves whose directions span a substantial fraction of the mean Bragg angle. Such off Bragg waves can be handled via the same technique as above, but one must use fractional-order Mathieu functions [9,10]. These functions have characteristic-value curves that lie in the so-called stable regions of the characteristic value chart of Fig. 4. Second, the sharp-edged boundary may not apply. In general, a soft-edged boundary calls for a z-dependent q. Third, if the detuning of the light is small (or zero), the potential is complex (or imaginary) and hence at least partially absorbing [13]. Mathieu functions do exist for complex q [10]. Fourth, the potential can be made time dependent [14]. Theoretical consideration of these situations will be presented elsewhere. However, it seems clear that in these extensions the products of Mathieu functions and characteristic exponentials in z will play a central role since these are the base states in a sinusoidal medium.

ACKNOWLEDGMENTS

This work was supported by the National Science Foundation under Grant No. PH97-22614, the Austrian Science Foundation (FWF) under Project No. S 6504, and the Austrian-Czech Cooperation Agreement (Aktion) under Project No. 18p2/1998.

[1] P. M. Morse, Phys. Rev. **35**, 1310 (1930).
[2] M. V. Laue, Phys. Rev. **37**, 53 (1931).
[3] L. Brillouin and M. Parodi, *Propagation des Ondes Dans les Millieux Périodiques* (Masson and Dunod, Paris, 1956).
[4] P. J. Martin, B. G. Oldaker, A. H. Miklich, and D. E. Pritchard, Phys. Rev. Lett. **60**, 515 (1988).
[5] D. O. Chudesnikov and V. P. Yakovlev, Laser Phys. **1**, 110 (1991).
[6] H. Rauch and D. Petrascheck, in *Neutron Diffraction*, edited by H. Dachs (Springer, Berlin, 1978).
[7] J. Arthur and M. A. Horne, Phys. Rev. B **32**, 5747 (1985).
[8] M. A. Horne, K. D. Finkelstein, C. G. Shull, A. Zeilinger, and H. J. Bernstein, Physica B **151**, 189 (1988).
[9] N. W. McLachlan, *Theory and Application of Mathieu Functions* (Dover, New York, 1964).
[10] J. Meixner and F. W. Schäfke, *Mathieusche Funktionen und Sphäroidfunktionen* (Springer-Verlag, Berlin, 1954).
[11] M. S. Chapman, C. R. Ekstrom, T. D. Hammond, J. Schmiedmayer, B. E. Tannian, S. Wehinger, and D. E. Pritchard, Phys. Rev. A **51**, R14 (1995).
[12] A recent overview of atom optics and interferometry can be found in *Atom Interferometry*, edited by P. R. Berman (Academic, New York, 1997).
[13] M. K. Oberthaler, R. Abfalterer, S. Bernet, J. Schmiedmayer, and A. Zeilinger, Phys. Rev. Lett. **77**, 4980 (1996).
[14] S. Bernet, M. K. Oberthaler, R. Abfalterer, J. Schmiedmayer, and A. Zeilinger, Phys. Rev. Lett. **77**, 5160 (1996).